# Evaluation of Adhesion Strength of $Er_2O_3$ Coating Layer for an Advanced Breeding Blanket System Applied to Thermal Cycles using Nano-Scratch Method

Yoshimitsu HISHINUMA, Teruya TANAKA, Kenji MATSUDA[1)], Daisuke TAKADA[2)], Toshihiro HOSEN[2)], Akio SAGARA and Takeo MUROGA

*National Institute for Fusion Science, Toki, Gifu 509-5292, Japan*
[1)]*University of Toyama, Toyama 903-8555, Japan*
[2)]*RHESCA Co.,Ltd, Hino, Tokyo 191-0011, Japan*

(Received 7 August 2013 / Accepted 1 December 2013)

The electrical insulator and hydrogen permeation barrier coatings are important materials to realize the liquid metal and molten-salt typed breeding blanket systems. We found that erbium oxide ($Er_2O_3$) is one of the promising materials as the electrical insulator and hydrogen permeation restraint coatings. Establishing the mechanical property evaluation method for these coating is extremely important to certify the durability of coating material in the blanket systems. The adhesion strength property, which is one of the key mechanical properties of coating materials, was investigated using the nano-scratch method. From the results, it was found that the nano-scratch test was able to evaluate the adhesion strength of the $Er_2O_3$ coating synthesized by the Metal Organic Chemical Vapor Deposition (MOCVD) process with high reproducibility. Furthermore, the adhesion strength of the $Er_2O_3$ coating before and after thermal cycling was evaluated using this method. The adhesion strength after 50 thermal cycles at 700°C was kept around 70% compared with that before thermal cycling.



Keywords: blanket system, $Er_2O_3$ coating, scratch test, adhesion strength, thermal cycling

DOI: 10.1585/pfr.9.1405004

## 1. Introduction

In the magnetic confinement fusion reactor as the sustainable energy source, an advanced breeding blanket is perferable system to realize high energy conversion efficiency and high tritium breeding ratio (TBR). The liquid metal (Li and Pb-Li) and molten-salt (FLiBe and FLiNaK) typed breeding blankets are promising as advanced blanket systems. However, critical problems of these systems were pointed out for the application to the magnetic confinement fusion reactors. These include restraints by the Magneto Hydrodynamic (MHD) pressure drop for Li and Pb-Li systems, and the tritium permeation leakage for Pb-Li and molten-salt systems, respectively [1, 2]. An electrically insulating coating with ceramics material such as oxides and nitrides is one of the attractive methods to break off electromagnetic force inducing the MHD pressure drop. D.L. Smith *et al.* reported that modest electrical resistivity of $10^4\,\Omega$m is required in order to restrain the MHD pressure drop in the thin coating below 1 μm [3]. A coating with ceramic materials will also be effective to suppress to 1/1000 the hydrogen permeation from molten-salt such as FLiBe and FLiNaK [4]. These ceramic coating materials will be absolutely necessary to realize the various advanced blanket systems such as liquid Li, Pb-Li and molten-salt typed systems.

Some ceramic materials such as CaO, $Y_2O_3$, $CaZrO_3$, AlN and $Er_2O_3$ have been studied as the candidate materials for the insulating coating [5, 6]. $Er_2O_3$ was selected as one of the candidate materials for the insulator coating for reducing the MHD pressure drop because of high compatibility with liquid Li and high electrical resistivity at higher temperature [6]. Furthermore, it was found that $Er_2O_3$ layer can significantly suppress hydrogen permeation. Thus, we are convinced that $Er_2O_3$ is a suitable coating material as not only the electrical insulator but also tritium leakage barrier materials. Various technologies have therefore been developed for coating $Er_2O_3$ layer on blanket structural materials [6–9]. Chemical vapor deposition (CVD) is a potential method for large area of complex-shaped coating, and metal organic vapor deposition (MOCVD) process was applied as a new technology for $Er_2O_3$ coating on broad and complicated shaped components including duct interiors [10–13].

Characterization of the $Er_2O_3$ coating has been carried out by hardness and microstructure. Although adhesion to the substrate is one of the key properties of the ceramic coatings, systematic evaluation of the properties of $Er_2O_3$ coatings has not been carried out partly because the methodology of evaluation has not been established. To clarify adhesion strength of ceramic coating material under

*author's e-mail: hishinuma.yoshimitsu@nifs.ac.jp*

the blanket operation condition will contribute to the blanket design by providing estimate of soundness and durability of the coating as the blanket component material.

Generally, there are a few methods to evaluate the adhesion strengths of the soft coating materials such as the plated layer and polymer film, which are cross-cut adhesion and pull off methods [14, 15]. These methods are theoretically simple and easy technique, but these are not suitable for the hard coating materials such as PVD and CVD coating, because, in the cross-cut adhesion and pull off methods, it was very difficult to make small grid-shaped slit in the hard coating. In addition, the quantitative adhesion evaluation of multi-coating layer could not be carried out using cross-cut adhesion and pull off methods. Furthermore, these methods are only available when the adhesion strength of coating layer is weaker than that of the separation tape and bond.

In 1997, the scratch method was made applicable to the case which needs much larger external forces to separate from a substrate like the case of hard coating, and was qualified to the JIS R3255. In the nano-scratch method, a diamond stylus pressed on the surface of coating layer, scratched the surface of the coating layer with an increasing applied dynamic load. Using this scratch mechanism, the adhesion evaluation is possible on not only single layer but also multi-layered samples. Further advantage of the scratch method is that larger dynamic load can be applied to the hard coating layer compared with the cross-cut adhesion and pull off methods. This method has been applied to the inspection of the car paint-films, cutware tool and the diamond like carbon (DLC) film and so on [16].

In this paper, the adhesion strength measurement of MOCVD processed $Er_2O_3$ thin coating layer on the metal substrate was carried out using nano-scratch method for the purpose of establishing adhesion strength evaluation for thin coating layers. In this case, the stainless steel (SUS316) was used as the substrate for demonstrating the present technology using a well-characterized material instead of low activation candidate materials for fusion blanket such as Reduced Activation Ferritc/Martensitic Steel (RAFM), Oxide Dispersive Strengthen (ODS) steel and vanadium alloys. In addition, we also prepared the MOCVD processed $Er_2O_3$ coating after thermal cycles for several times between room temperature and 700°C in Ar atmosphere. The changes of microstructure and adhesion strength of $Er_2O_3$ coating layer by the thermal cycling were investigated.

## 2. Samples and Experimental Procedure

### 2.1 Preparation of MOCVD processed $Er_2O_3$ coating with thermal cycling

The $Er_2O_3$ coating layers were formed on SUS 316 disk plate using MOCVD apparatus in National Institute for Fusion Science (NIFS). The MOCVD apparatus in NIFS and the MOCVD process was described in detail in Refs. [10–13]. The dimension of SUS 316 disk is 17 mm in diameter and 1 mm in thickness. The deposition temperatures and time were fixed to 450, 475 and 500°C and 2 hours. Figure 1 shows typical optical image of MOCVD processed $Er_2O_3$ on SUS 316 substrate. The change of microstructure in $Er_2O_3$ coating layer was characterized by XRD analysis and SEM and TEM observations. According to the XRD pattern of the coating layer, all of main peaks were identified as a $Er_2O_3$ phase. TEM image of the cross-sectional area in $Er_2O_3$ coating layer via MOCVD process is shown in Fig. 2. The thickness of $Er_2O_3$ coating layer was about 700 nm. The layer was grown densely like columnar grain texture. In the boundary of $Er_2O_3$ and SUS 316 substrate, no macroscopic defect such as crack and separation was observed.

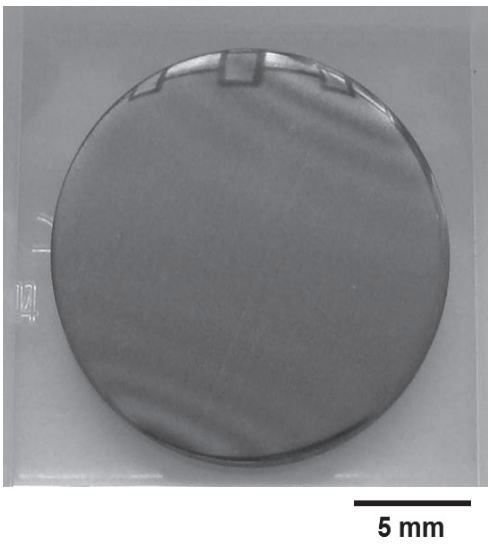


Fig. 1 Typical photograph of $Er_2O_3$ coating on SUS 316 substrate via MOCVD process.

Thermal cycling tests were carried out for some samples. The thermal cycling temperature was fixed at 700°C. This temperature was assumed as the operation condition of the liquid metal blanket systems such as Li [17] and Pb-Li [18]. The samples were set into the temperature plateau region of the electrical furnace and were heated up to 700°C of the peak temperature under Ar gas flowing. The temperature was elevated to peak temperature at a rate of 700°C/hour and then held for 1 hour, followed by furnace cooling to 50°C. The number of thermal cycling was 10, 30 and 50. Figure 3 shows typical temperature history during 30 times of the thermal cycling.

The changes of microstructure and adhesion strength on the MOCVD processed $Er_2O_3$ coating on SUS 316 substrate after the thermal cycling were also investigated using the XRD analysis, SEM and TEM observations and the nano-scratch test.

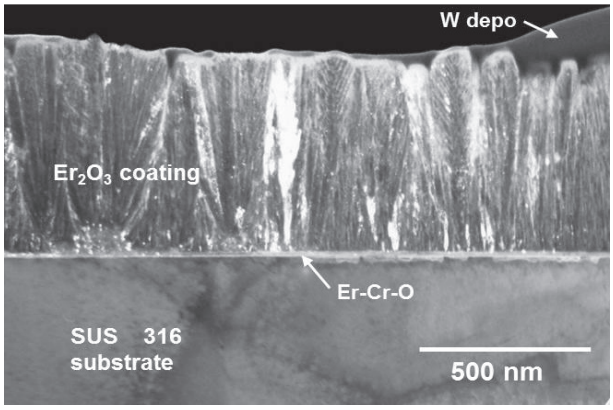


Fig. 2 TEM image of cross-sectional area in $Er_2O_3$ coating layer on SUS 316 substrate via MOCVD process.

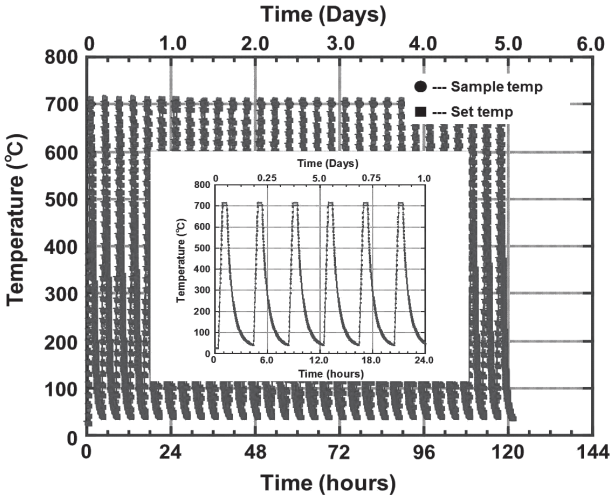


Fig. 3 Temperature history of the $Er_2O_3$ coating sample during 30 times of thermal cycling.

## 2.2 The measurement principle of the nano-scratch method

In order to evaluate adhesion strength of the MOCVD processed $Er_2O_3$ coating samples before and after thermal cycling, nano-scratch tests were carried out using nano-layer scratch instrument (CSR-2000: RHESCA Co.,Ltd). The configuration and interaction between the diamond scratch stylus tip and surface of coating layer is shown in Fig. 4. In these tests, the surface of the coating layer is scratched by a vibrating diamond stylus tip of a given curvature radius mounted on an elastic arm while the stylus is being lowered in the coating thickness direction. The elastic arm is deformed because of the lowering movement of the stylus, resulting in an increased load force to the coating layer applied by the stylus.

According to the formula of Benjamin and Weaver, the relationship between the dynamic load ($W$) applied by the stylus to the coating and the shearing stress ($F_s$) on the interface the coating layer and substrate have established

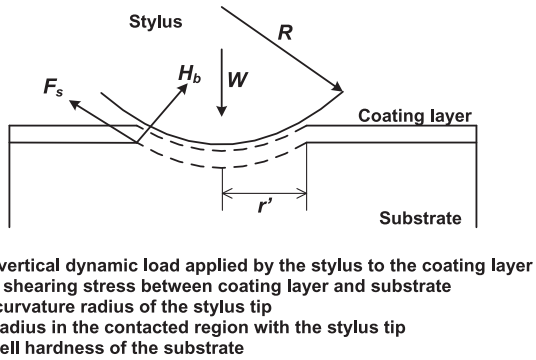


Fig. 4 The configuration and interaction between the diamond scratch stylus and surface of the coating layer.

as the following Eq. (1) [19],

$$F_s = H_b / \sqrt{(\pi R^2 H_b / W) - 1}, \quad (1)$$

where $R$ is the curvature radius of the stylus, and $H_b$ indicates Brinell hardness of the substrate. As the dynamic load to the coating ($W$) is increased, the shearing stress ($F_s$) on the boundary between coating and substrate increases. When the shearing stress exceeds the adhesive strength of the coating layer, the coating layer on the substrate is broken and/or separated from the substrate. This minimum dynamic load when the coating layer breaks and/or separates from the substrate is defined as the critical adhesion force ($Wc$) in this study.

The schematic image of the scratch mechanism and the photograph of practical sample setting on X-Y stage of nano-scratch instrument are shown in Figs. 5 (a) and (b). The nano-scratch instrument uses the following procedure to detect the coating adhesion. A stylus, which is mounted on a cartridge vibrating in the Y direction, is pressed against a coating. Then, the friction generated between the stylus and the coating causes the stylus to lag slightly behind the motion of the cartridge, and the relative position is changed between the magnet mounted on the elastic arm and the coil installed in the cartridge. Thus, electrical output is produced from the cartridge. When the coating fracture occurs, the electrical output will change due to the fluctuation of friction coefficient or patterned indented coating surface. This change in electrical output is used to detect the coating fracture, and the critical force at the time of adhesion and fracture is calculated (the load force value at the time of fracture refers to the critical fracture force, $Wc$).

The nano-scratch measurement conditions in the present study are as follows; excitation width of stylus is 100 μm, curvature radius of stylus is 15 μm, elastic arm constant is 100 g/mm and scratch measurement speed is 10 μm/sec.

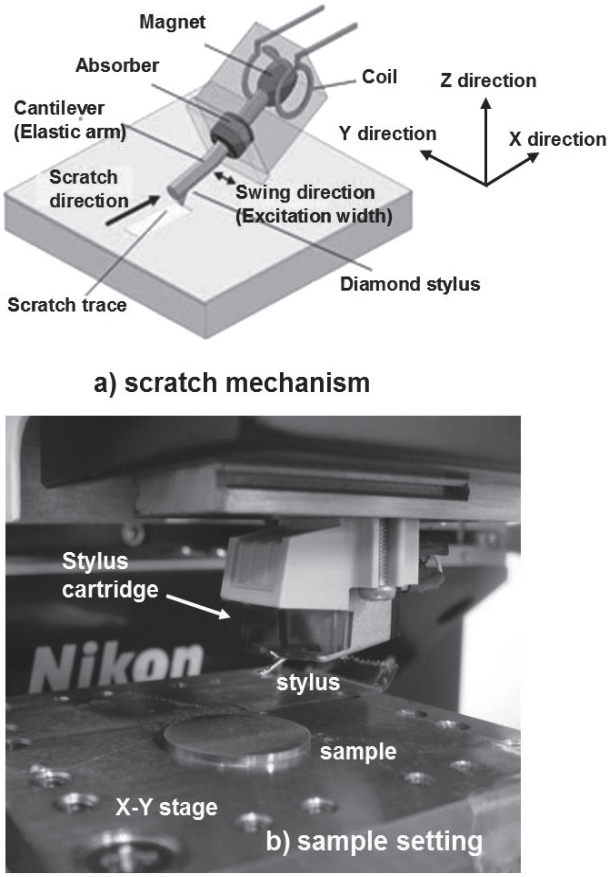


Fig. 5 The schematic image of the scratch mechanism and the photograph of practical sample setting on X-Y stage of nano-scratch instrument. (a) The schematic image of scratch mechanism and (b) The coating sample on the X-Y stage of nano-layer scratch instrument.

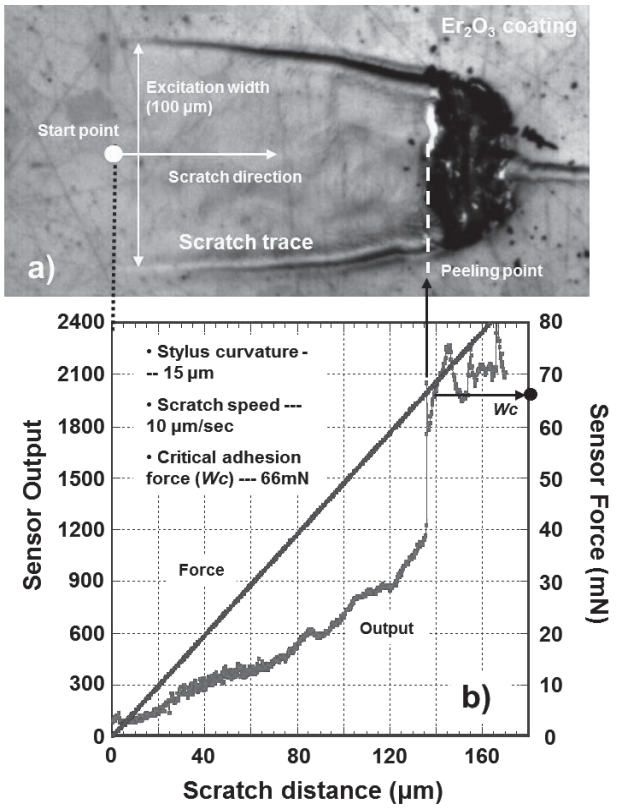


Fig. 6 Typical scratch trace image and test data of $Er_2O_3$ coating layer using the nano-layer scratch instrument. (a) The CCD image of the nano-scratch trace on the $Er_2O_3$ coating layer and (b) the displacement diagram between sensor output and force.

# 3. Results

## 3.1 The adhesion strength of MOCVD processed $Er_2O_3$ coating layer on SUS 316 substrate

Typical scratch trace image and test data of $Er_2O_3$ coating layer using nano-layer scratch instrument are shown in Figs. 6 (a) and (b). The scratch trace image was taken by CCD camera attached to the nano-layer scratch instrument. We found that the scratch trace corresponded with the displacement diagram between the sensor output and the applied scratch force. The excitation amplitude of the stylus became smaller with the increase in the applied scratch force. At the same time, the sensor output was also increased with the decrease in the excitation amplitude. Here, the sensor output indicates friction force between the stylus and coating surface. On the other hands, the sensor output was increased with increasing applied scratch force and the significant increase of sensor output coincided with the separation point of the scratch trace. We defined the applied force at the significant increase of sensor output as the critical adhesion force (*Wc*). In this way, nano-layer scratch instrument is available to evaluate the adhesion strength of the MOCVD processed $Er_2O_3$ thin coating.

The relationship between formation temperature and the adhesion strength on the MOCVD processed $Er_2O_3$ thin coating was investigated. The critical adhesion strength (*Wc*) as a function of the substrate temperature during synthesis of the $Er_2O_3$ layer by the MOCVD process is shown in Fig. 7. Seven pieces of the coated samples were tested at each temperature. The nano-layer scratch test was carried out at randomly selected three points per one sample, and the adhesion strength was estimated by the average value of the three points. The average adhesion strength of $Er_2O_3$ coating layer changed from 79 mN to 64 mN with increasing substrate temperature during the MOCVD process. At all substrate temperatures tested, a Er-Cr-O compound layer was observed around interface between the $Er_2O_3$ coating and the SUS 316 substrate as shown in Fig. 2. The formation of the Er-Cr-O compound layer was caused by the Cr diffusion from the SUS substrate, and the thickness of Er-Cr-O layer was estimated to be about 15~20 nm.

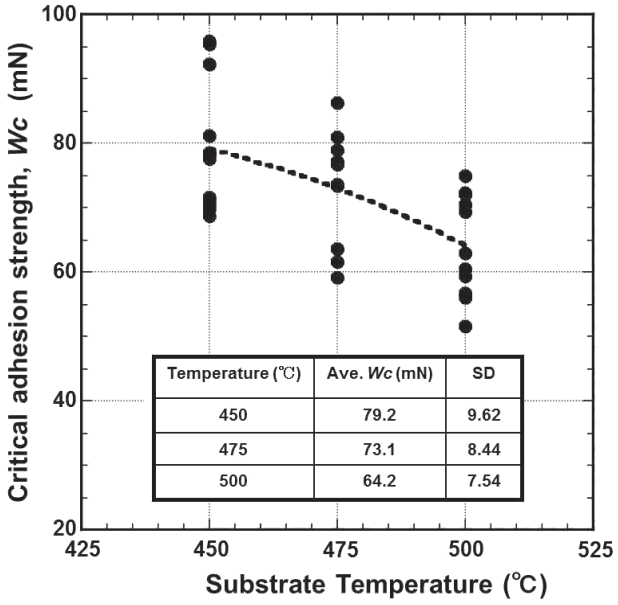


Fig. 7 The critical adhesion strength (*Wc*) as a function of the substrate temperature during the synthesis of $Er_2O_3$ coating with MOCVD process.

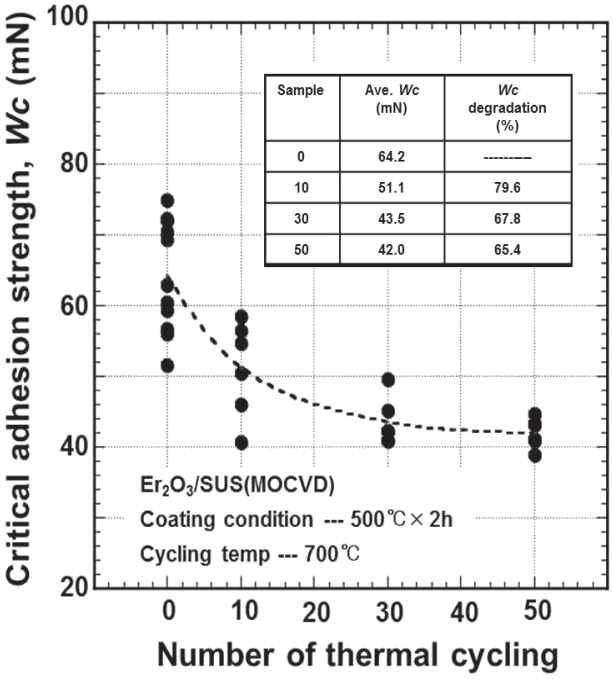


Fig. 8 The critical adhesion strength (*Wc*) as a function of the number of times of heat-cycling in the $Er_2O_3$ coating layer synthesized with MOCVD process.

## 3.2 The changes of adhesion strength and microstructure of $Er_2O_3$ coating layer by the thermal cycling

The critical adhesion strength (*Wc*) as a function of the number of thermal cycles is shown in Fig. 8. Similar to Fig. 7, seven coated samples at three points each were tested for a thermal cycling condition. The adhesion strength of $Er_2O_3$ coating layer decreased with increasing the number of thermal cycles from 64.1 mN (Original sample) to 51.1 mN (10 times), 44.5 mN (30 times) and 44.2 mN (50 times). It is to be noted that the adhesion strength between 30 and 50 times of thermal cycling are similar to each other. This means that the adhesion strength property was saturated with the number of thermal cycles.

On the other hand, the change of texture on the $Er_2O_3$ coating was investigated using XRD analysis. XRD patterns of the $Er_2O_3$ coating layer as a function of number of thermal cycling are shown in Fig. 9. We found that the $Er_2O_3$ texture before thermal cycling was oriented randomly in the coating layer without alignment texture. However, the peak intensity of (400) plane of $Er_2O_3$ phase after 50 times of thermal cycling was drastically increased. The peak intensity ratio such as (400)/(222) shown in Fig. 9 was also remarkably increased from 1.52 to 80.62 with 50 thermal cycles. This means that a-axis alignment was promoted by the thermal cycling on the $Er_2O_3$ coating. In addition, the comparison between the rocking curves of (400) plane on $Er_2O_3$ phase ($2\theta$ = 33.97 deg.) before and after the thermal cycling is shown in Fig. 10. The Full Width at Half Maximum (FWHM) value of (400) plane on $Er_2O_3$ phase was decreased from 13 to 9.5 by the thermal cycling.

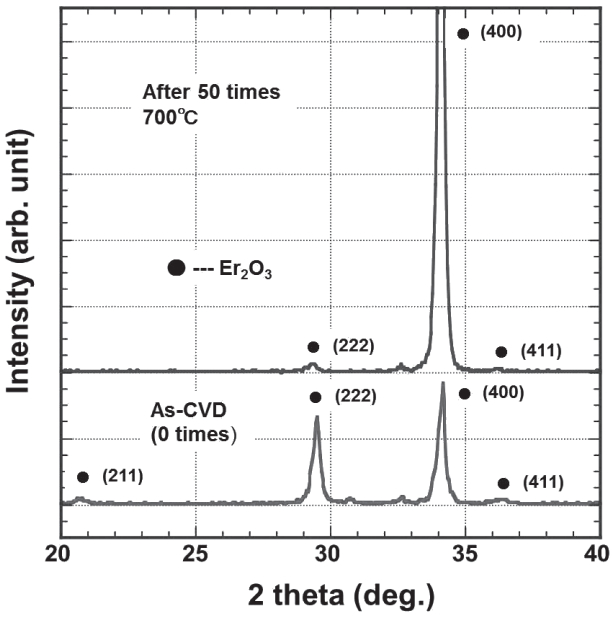


Fig. 9 XRD patterns of $Er_2O_3$ coating layer synthesized with MOCVD process before and after the thermal cycling.

This suggests that the crystallinity of $Er_2O_3$ was improved by the thermal cycling

Typical TEM image of the cross-sectional area in the interface between the $Er_2O_3$ coating layer and substrate after 30 thermal cycling is shown in Fig. 11. As same as Fig. 2, Er-Cr-O compound layer was clearly confirmed. The thickness of Er-Cr-O compound layer was estimated

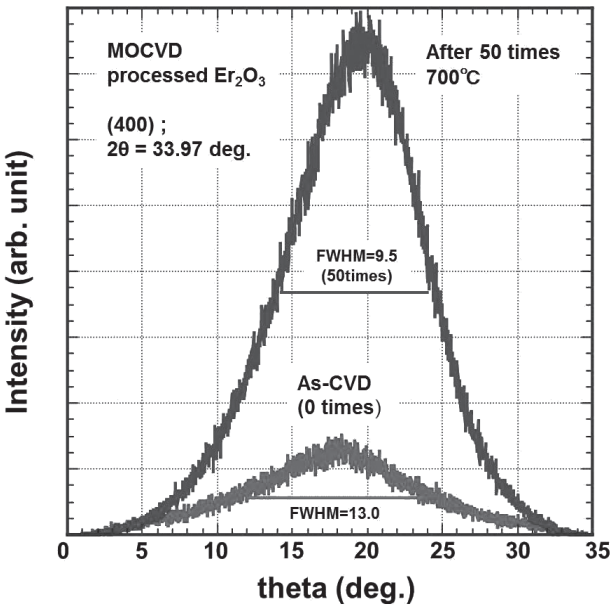


Fig. 10 The comparison between the rocking curves of (400) plane on $Er_2O_3$ phase ($2\theta = 33.97°$) before and after the thermal cycling.

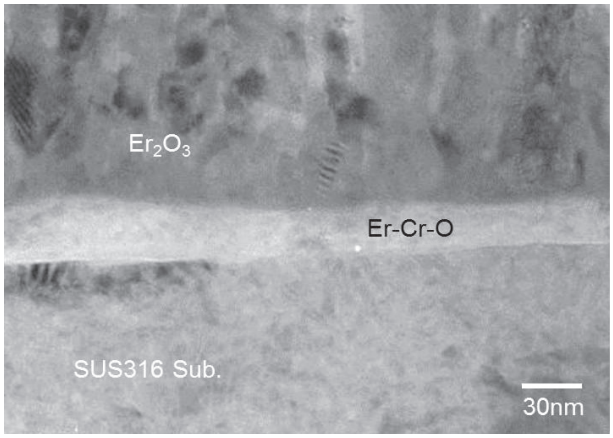


Fig. 11 TEM image of the cross-sectional area in the interface between $Er_2O_3$ coating layer and SUS 316 substrate after 30 thermal cycling.

to about 30~40 nm. Thicker Er-Cr-O compound layer was formed compared with that before the thermal cycling shown in Fig. 2. These suggested that the Cr diffusion from SUS substrate was promoted by the thermal cycling and the increase of thickness on Er-Cr-O compound layer was caused by the enhanced Cr diffusion.

## 4. Discussions

In this study, the change of adhesion strength (*Wc*) of $Er_2O_3$ ceramic coating by the thermal cycling was investigated using nano-scratch method. The change would become one of the key factors for applying the coating to advanced breeding blanket system, potentially contributing to the design of maintenance schedule and the exchange scenario. From the results of nano-scratch tests, we found that the adhesion strength (*Wc*) of the $Er_2O_3$ coating layer after 50 thermal cycles at 700°C was kept stably about 70 % of that for as-CVD coated samples. Here, in the case of Force Free Helical Reactor (FFHR) design in NIFS, the life-time design of blanket system is 30 years [20–22]. If the maintenance of blanket system is carried out once a year, major thermal cycling of more than 30 times is expected during the life-time of blanket system. The degradation of adhesion strength shown in Fig. 8 was saturated between from 30 to 50 times of thermal cycling. Thus, it is suggested that $Er_2O_3$ coating synthesized with MOCVD process have significant mechanical durability throughout the blanket life time.

The change of microstructure of $Er_2O_3$ by the thermal cycling characterized using XRD analysis, SEM and TEM observations is also discussed. From the comparisons of XRD patterns before and after thermal cycling shown in Fig. 9, we found that lattice parameter of $Er_2O_3$ crystal estimated from XRD peaks was not changed by the thermal cycling. In addition, microstructure of the $Er_2O_3$ coating layer was changed from random texture (non-alignment) to a-axis alignment texture. As reported in [13], the peak intensity ratio of (400)/(222) plane after 30 times of thermal cycling was obtained to 7.2. Thus, a-axis alignment was promoted by thermal cycling. Generally, FWHM value estimated by the rocking curve shown in Fig. 10 indicates the degree of crystallintiy, and FWHM after the thermal cycling was decreased compared with that of as-MOCVD sample. This implies that the crystallinity of $Er_2O_3$ was improved by thermal cycling. These suggested that $Er_2O_3$ phase was maintained without the phase transformation during the thermal cycling and a-axis grain growth with enhanced $Er_2O_3$ crystallinity was promoted by the thermal cycling. From the comparisons of microstructure around the interface of the coating and substrate by the thermal cycling shown in Fig. 11, we found that the Er-Cr-O compound layer thickness was increased from 20 μm to 40 μm after the thermal cycling. This was caused by the Cr diffusion from SUS substrate promoted by the thermal cycling.

Effective factors to cause *Wc* degradation by the thermal cycling is considered. Generally, the change of microstructure and the residual stress around the interface of coating and substrate are relatively effective factors of coating separation from substrate. In our study, we confirmed that in some cases perpendicular cracks between $Er_2O_3$ columnar crystals were formed after thermal cycling. This will be caused by the different coefficient of thermal expansion. The average coefficient of thermal expansion of SUS 316 ($18.5\times10^{-6}$°$C^{-1}$) was about 2.5 times larger compared with that of $Er_2O_3$ ($7.25\times10^{-6}$°$C^{-1}$). The formation of perpendicular crack will also become one of the factors to cause *Wc* degradation by thermal cycling.

On the other hands, the residual stress around interface between coating and substrate is considered. The

residual stress around interface between coating and substrate by the thermal cycling is estimated by the equation based on the thermal stress as [23],

$$S = E_{\mathrm{f}}(\alpha_{\mathrm{f}} - \alpha_{\mathrm{s}})\Delta T d, \quad (2)$$

where $S$ is residual stress around interface, $E_{\mathrm{f}}$ is Young's modulus of coating, $\alpha_{\mathrm{f}}$ and $\alpha_{\mathrm{s}}$ are the coefficient of thermal expansion of coating and substrate, $\Delta T$ is the change of the temperature on the thermal cycling and $d$ is coating thickness, respectively. According to the Eq. (2), the residual stress is the proportional to the coating thickness. Increase of Er-Cr-O compound layer thickness shown in Fig. 11 would cause an increase of residual stress around the interface between coating and substrate. The interfacial fracture as a result of the increased stress between Er-Cr-O layer and substrate will be the origin of the coating separation from the substrate.

In addition, the enhancement of a-axis alignment by the thermal cycling shown in Fig. 9 is investigated. Adel A. Sharif et al reported that Young's modulus of $Er_2O_3$ single crystal is 150 and 183 GPa in (100) and (111) plane, respectively [24]. Thus, according to Eq. (1), the residual stress is considered to decrease by the enhancement of a-axis alignment. Therefore, we thought that the formation of the perpendicular cracks and increase of Er-Cr-O layer thickness will be mainly effective reasons to cause the *Wc* degradation by the thermal cycling. Furthermore, the enhancement of $Er_2O_3$ cystallization by the high thermal cycling shown in Fig. 10 promotes change from diversely oriented small phases to a homogeneous $Er_2O_3$ crystal which is thought to results in the decreased error bar shown in Fig. 9.

The expandability of nano-scratch test in mechanical property evaluation of ceramic coating as the advanced blanket component is examined. In the scratch test, the surface of the coating layer is scratched by a vibrating diamond stylus of a given curvature radius mounted on an elastic arm while the stylus is being lowered in the coating thickness direction. The coating layer was ground by vibrating diamond with increasing dynamic load during the scratch test. Then, we propose the scratch test is able to apply to the abrasion evaluation as well. With constant dynamic load applied to the coating with a constant thickness, the output of the scratch sensor as a function of time provides abrasion characteristics of the coating. The time at the significant increase of sensor output is defined as the critical abrasion time. It is thought that the change of abrasion property can be extracted using the scratch time as the parameter.

# 5. Conclusions

We investigated adhesion strength of $Er_2O_3$ coating using nano-scratch instrument for application to advanced breeding blanket components. The adhesion strength of $Er_2O_3$ coating layer could be evaluated with reproducibility by nano-scratch method.

The adhesion strength of $Er_2O_3$ coating layer decreased with the increase in the thermal cycling and the adhesion strength degradation was limited to about 70 % of the original $Er_2O_3$ coating layer. We found that $Er_2O_3$ coating synthesized with MOCVD process have significant mechanical durability and would survive the expected thermal cycling during the life-time of blanket systems. From the comparisons of microstructure and residual stress based on the thermal stress after the thermal cycling, the formation of the perpendicular cracks and increase of Er-Cr-O layer thickness around interface will be the main effective reasons to cause the adhesion strength degradation by the thermal cycling.

# Acknowledgments

This work was mainly supported by the Fusion Engineering Research Project in NIFS (UFFF026), and in part by the NIFS Collaboration Research Program (KEMF045).

[1] S. Malang, H.U. Borgstedt, E.H. Farnum, K. Natesan and I.V. Vitkovski, Fusion Eng. Des. **27**, 570 (1995).
[2] T. Muroga, T. Tanaka and A. Sagara, Fusion Eng. Des. **81**, 1203 (2006).
[3] D.L. Smith, K. Natesan, J.-H. Park, C.B. Reed and R.F. Mattas, Fusion Eng. Des. **51–52**, 185 (2000).
[4] T. Tanaka, Y. Hirooka and S. Fukada, J. Plasma Fusion Res. **89**, 384 (2013) (in Japanese).
[5] D.L. Smith, J. Konys, T. Muroga and V. Evtikhin, J. Nucl. Mater. **307–311**, 1314 (2002).
[6] B.A. Pint, P.F. Tortorelli, A. Jankowski, J. Hayes, T. Muroga, A. Suzuki, O.I. Yeliseyeva and V.M. Chernov, J. Nucl. Mater. **329–333**, 119 (2004).
[7] A. Sawada, A. Suzuki, H. Maier, F. Koch, T. Terai and T. Muroga, Fusion Eng. Des. **75–79**, 737 (2005).
[8] X. Li, P. Wu, H. Qiu, S. Chen and B. Song, Thin Solid Film **520**, 2316 (2012).
[9] D. Zhang, M. Kondo, T. Tanaka, T. Muroga and T. Valentyn, Fusion. Eng. Des. **86**, 2508 (2011).
[10] Y. Hishinuma, T. Tanaka, T. Tanaka, T. Nagasaka, Y. Tasaki, A. Sagara and T. Muroga, Fusion. Eng. Des. **86**, 2530 (2011).
[11] Y. Hishinuma, T. Tanaka, T. Tanaka, T. Nagasaka, S. Yoshizawa, Y. Tasaki and T. Muroga, J. Nucl. Mater. **417**, 1214 (2011).
[12] Y. Hishinuma, T. Tanaka, T. Tanaka, T. Nagasaka, Y. Tasaki, S. Murakami, K. Matsuda, A. Sagara and T. Muroga, Fusion Sci. Technol. **60**, 1131 (2011).
[13] Y. Hishinuma, S. Murakami, K. Matsuda, T. Tanaka, Y. Tasaki, T. Tanaka, T. Nagasaka, A. Sagara and T. Muroga, Plasma Fusion Res. **7**, 2405127 (2012).
[14] K. De Bruyn, M. Van Stappen, H. De Deurwaerder, L. Rouxhet and J.P. Celis, Surf. Coat. Technol. **163–164**, 710 (2003).
[15] Jeong-Gi Jin, Sung-Ki Lee and Young-Ho Kim, Thin Solid Films **466**, 272 (2004).
[16] S. Miyake, T. Saitoh, S. Watanebe, M. Kanou, Y. Yasuda and Y. Mabuchi, Tribologist **45**, 469 (2000) (in Japanese).
[17] F. Najmabadia and the ARIES Team, Fusion. Eng. Des. **38**,

3 (1997).
[18] L. EI-Gueebaly and the ARIES Team, Fusion. Eng. Des. **51–52**, 325 (2000).
[19] P. Benjamin and C. Weaver, Proc. R. Soc. London Ser. A **254**, 163 (1960).
[20] A. Sagara, H. Yamanishi, T. Uda, O. Motojima, O. Mitarai, T. Kunugi, Y. Matsumoto, S. Satake, Y. Wu, T. Terai, S. Tanaka, H. Matsui, S. Takahashi, T. Yamamoto, S. Toda, S. Fukada, M. Nishikawa, A. Shimizu and N. Yoshida, Fusion. Technol. **39**, 753 (2001).
[21] A. Sagara, S. Imagawa, O. Mitarai, T. Dolan, T. Tanaka, Y. Kubota, K. Yamazaki, K.Y. Watanabe, N. Mizuguchi, T. Muroga, N. Noda, O. Kaneko, H. Yamada, N. Ohyabu, T. Uda, A. Komori, S. Sudo and O. Motojima, Nucl. Fusion **45**, 258 (2005).
[22] T. Tanaka, T. Muroga and A. Sagara, Fusion Sci. Technol. **47**, 530 (2005).
[23] M. Imaoka, Ann. Report of Tottori Institute for Industrial Technology **14**, 1 (2011) (in Japanese).
[24] A.A. Sharif, F. Chu, A. Misra, T.E. Mitchell and J.J. Petrovic, J. Am. Ceram. Soc. **83**, 2246 (2000).